Supporting Information for "Deformational-energy partitioning in glacier shear zones"

Meghana Ranganathan[1], Brent Minchew[1], Colin R. Meyer[2], Matěj Peč[1]

[1]Department of Earth, Atmospheric and Planetary Sciences, Massachusetts Institute of Technology, Cambridge, MA, USA

[2]Thayer School of Engineering, Dartmouth College, Hanover, NtH, USA

Contents of this file

———

July 15, 2021, 1:45pm

:

1.   Conservation of Energy

The first law of thermodynamics is

$$\dot{U} = \dot{Q} + \dot{W} \tag{1}$$

where $\dot{U}$ is the rate of change of internal energy, $\dot{Q}$ is the rate of change of energy supplied through heat, and $\dot{W}$ is the rate of work done on volume Ω by the surrounding material. The rate of change of internal energy can be found by:

$$\dot{U} = \frac{D}{Dt} \int_{\Omega} (\rho c_p T + \frac{1}{2}\rho u_i u_i + E_{\text{non-thermal}})dV \tag{2}$$

where $\frac{D}{Dt}$ is the material derivative, c_p is the specific heat capacity of ice, T is ice temperature, u_i is the velocity of the ice, $\rho c_p T$ is the thermal energy, and $\frac{1}{2}\rho u_i u_i$ is the kinetic energy and where repeating indices indicate summation. As defined in Ranganathan et al. (2021), $E_{\text{non-thermal}}$ can be approximated by the change in energy due to recrystallization, assuming recrystallization is the dominant mechanism altering the strain and surface energy state of the ice, such that $\dot{E}_{\text{non-thermal}} = \dot{E}_{\text{surface}} - \dot{E}_{\text{strain}}$, in which $\dot{E}_{\text{surface}}$ is the rate of change of surface energy during rotation recrystallization and $\dot{E}_{\text{strain}}$ is the rate of change of strain energy during migration recrystallization, with the overdot denoting a time derivative. Both E_{surface} and E_{strain} can be found by considering the grain size and dislocation density within the grains, such that

$$\dot{E}_{\text{surface}} - \dot{E}_{\text{strain}} = \frac{c\gamma}{d} - \frac{1}{2}\left(\frac{D}{d}\right)^{\frac{p}{2}}\frac{\tau_s^2}{\mu} \tag{3}$$

where p is the grain-growth exponent, D is the characteristic length-scale, τ_s is the shear stress, and d is the grain size. The full derivation is found in Ranganathan et al. (2021).

The rate of heat transfer by conduction can be found from Fourier's Law as

$$\dot{Q} = -\int_{\partial\Omega} KT_{,j}(-n_j)ds \tag{4}$$

where K is the thermal conductivity. The rate of work done by the surrounding material is

$$\dot{W} = -\int_{\partial\Omega} \tau_{ij}u_i(-n_j)ds + \int_{\Omega} \rho g_i u_i dV \tag{5}$$

In this study, we assume incompressibility and we neglect kinetic energy, as we are in a low Reynolds number regime and therefore kinetic energy is likely to be negligible. Thus, internal energy U is approximately equivalent to enthalpy H such that Equation 2 can be written in terms of enthalpy as

$$H = \rho c_p T + \frac{c\gamma}{d} - \frac{1}{2}\left(\frac{D}{d}\right)^{\frac{p}{2}} \frac{\tau_s^2}{\mu} + H_0 \tag{6}$$

where H_0 is a constant offset. From the first law of thermodynamics, writing in terms of enthalpy, we get

$$\dot{U} = \dot{Q} + \dot{W} \tag{7}$$

$$\implies \frac{D}{Dt}\int_{\Omega} HdV = -\int_{\partial\Omega} KT_{,j}(-n_j)ds + -\int_{\partial\Omega} \tau_{ij}u_i(-n_j)ds \tag{8}$$

$$\implies \int_{\Omega} \frac{DH}{Dt}dV = \int_{\Omega}(KT_{,j} + \tau_{ij}u_i)_{,j}dV \tag{9}$$

$$\implies \frac{DH}{Dt} = (KT_{,j})_{,j} + \tau_{ij}u_{i,j} \tag{10}$$

Equation 10 can be rewritten as

$$\frac{\partial H}{\partial t} + \underline{u} \cdot \nabla H = K\nabla^2 T + \tau_{ij}\dot{\epsilon}_{ij} \tag{11}$$

in which the material derivative of enthalpy is the sum of the enthalpy flux and the work put into the system by deformation. Equation 11 is the conservation of energy equation, in which internal energy is a sum of change of energy from heat and the change in energy due to work being done on the volume. This balance relates the change in surface, strain, and thermal energy to the work rate. We can partition Equation 11 into:

$$\frac{c\gamma}{d} - \frac{1}{2}\left(\frac{D}{d}\right)^{\frac{p}{2}}\frac{\tau_s^2}{\mu} = (1-\Theta)\tau_{ij}\dot{\epsilon}_{ij} \tag{12a}$$

$$\rho c_p \left(\frac{\partial T}{\partial t} + \underline{u} \cdot \nabla T\right) = K\nabla^2 T + \Theta\tau_{ij}\dot{\epsilon}_{ij} \tag{12b}$$

where Equation 12a is the non-thermal energy component found from Equation 3 and Equation 12b is the thermal energy component (also known as the evolution of temperature equation). This relates the change in thermal energy (left hand side) to the change in heat through heat conduction and the change in heat that originates from viscous dissipation ($\Theta\tau_{ij}\dot{\epsilon}_{ij}$). For the purposes of ice-flow models, we generally neglect firn compaction, air movement through firn, and melting/refreezing. In the case of this model, we also neglect geothermal heat, as we are most interested in how heat generated during the deformation and movement of ice affects ice flow, since these may provide positive feedbacks that amplify the effects during ice flow. Meyer & Minchew (2018) previously derived a thermomechanical model from this energy balance to estimate ice temperature in shear margins of Antarctic ice streams. The study presented here follows their model and the

assumptions from their model, including that there is no vertical shear. In other words, the strain rates are constant throughout the ice column and the ice slips along its bed. This implies that basal drag is negligible compared to drag along the lateral margins of the ice streams. Therefore, the primary heat source would be viscous dissipation during deformation.

While some fraction Θ of the mechanical work put into the ice during deformation gets converted into thermal energy, which is then advected or diffused, the remainder of the work gets converted into strain energy. Deformation increases the density of dislocations, which increases the strain energy state of ice (De La Chapelle et al., 1998). As the density of dislocations increases, the rate of deformation decreases due to pile-ups of dislocations preventing further creep (called work-hardening or strain-hardening) (Wilson & Zhang, 1996). Recovery mechanisms, including dynamic recrystallization, reduce the density of dislocations and allow for further creep. Recrystallization annihilates dislocations, either by the outward migration of grain boundaries, which destroy dislocations in their path (migration recrystallization), or by the subdivision of grains, during which new, strain-free grains are formed (rotation recrystallization) (Rollett & Kocks, 1993; Wenk et al., 1997; De Bresser et al., 1998; De La Chapelle et al., 1998; Montagnat & Duval, 2004).

Thus, during deformation, mechanical energy is converted to strain energy, and rotation recrystallization converts strain energy into surface energy, stored within grain boundaries (Derby & Ashby, 1987; Derby, 1992; De La Chapelle et al., 1998; Montagnat & Duval, 2000). Both mechanisms also destroy dislocation pileups, allowing dislocations to advect through dislocation creep, which functionally converts some of that strain energy back into mechanical energy. Finally, much of the strain energy is released during fracture events.

:

Therefore, as dislocations (and thus, strain energy) move with the strain-hardened ice downstream, eventually that energy is converted into surface energy during fracture and calving. We assume in this study that no other mechanisms are altering the energy state. It is unknown at the moment whether processes convert energy directly from surface and strain energy into heat, or whether all strain energy gets transferred back to mechanical energy or stored in grain boundaries or subgrain walls. Without further work suggesting otherwise, we assume this is not the case and reserve for future work an exploration of other mechanisms that may change the energy states.

However, the amount of mechanical energy converted to strain energy $(1 - \Theta)$ remains unknown. Constraining Θ is clearly necessary to fully understand the thermodynamics and energetics of ice flow and deformation, and thus the focus of this study is to constrain Θ.

2. Thermomechanical Model

Meyer & Minchew (2018) derived a thermomechanical model to compute ice temperature. Since their model only considered one column of ice, they simplified the heat equation to

$$-\rho c_p a \frac{\partial T}{\partial z} = K \frac{\partial^2 T}{\partial z^2} + \Theta \tau_{ij} \dot{\epsilon}_{ij} \tag{13}$$

where vertical velocity of ice $w = -a$ and lateral advection of ice is neglected. Note that they assumed $\Theta = 1$, and here we will rederive the model including this parameter Θ. The constitutive relation describing the flow of ice relates the stress to the strain rate as

$$\tau_{ij} = A^{\frac{-1}{n}} \left(\frac{1}{2} \dot{\epsilon}_{kl} \dot{\epsilon}_{kl} \right)^{\frac{1-n}{2n}} \tag{14}$$

July 15, 2021, 1:45pm

where n is the exponent in the constitutive relation commonly taken to be $n = 3$, from

borehole studies and laboratory measurements and A is the prefactor in the flow law,

also known as the flow rate parameter. A describes the dependence of viscosity to a

number of factors including temperature, fabric, porosity, liquid water content. From the

constitutive relation, we can then approximate

$$\Theta \tau_{ij} \dot{\epsilon}_{ij} = 2\Theta A^{-\frac{1}{n}} \dot{\epsilon}^{\frac{n+1}{n}} \tag{15}$$

where $\dot{\epsilon}$ is the lateral shear strain rate. We can further define two nondimensional numbers:

Brinkmann number represents the rate of dissipative heating to heat conduction:

$$Br = \frac{\Theta \tau_{ij} \dot{\epsilon}_{ij} H^2}{K \Delta T} \tag{16}$$

where ΔT is the difference between the melting temperature and the surface temperature,

and the Peclet number represents the ratio of accumulation to diffusion and is found as

$$Pe = \frac{\rho c_p a H}{K} \tag{17}$$

where a is accumulation and H is ice thickness. The critical shear strain rate to form a

temperate zone (a zone of temperate ice, heated by viscous dissipation) is

$$\dot{\epsilon}^* = \left(\frac{\frac{1}{2} Pe^2}{Pe - 1 + \exp\{-Pe\}} \right)^{\frac{n}{n+1}} \left[\frac{K \Delta T}{\Theta A^{\frac{-1}{n}} H^2} \right]^{\frac{n}{n+1}} \tag{18}$$

The thickness of this temperate zone is found by

$$\frac{\xi}{H} = \begin{cases} 1 - \frac{Pe}{Br} - \frac{1}{Pe}[1 + \mathcal{W}(-\exp\{-\frac{Pe^2}{Br} - 1\})], & \dot{\epsilon} > \dot{\epsilon}^* \\ 0, & \dot{\epsilon} \leq \dot{\epsilon}^* \end{cases} \quad (19)$$

where $f(\mathcal{W}) = \mathcal{W}e^{\mathcal{W}}$ is the product logarithm, i.e. the Lambert-W function. They then solve Equation 13 for ice temperature to find the following closed-form expression for ice temperature in the single column of ice:

$$T = \begin{cases} T_s + \Delta T \frac{Br}{2}[1 - \frac{z}{H} + \frac{1}{Pe}\exp\{Pe(\frac{\xi}{H} - 1)\} - \frac{1}{Pe}\exp\{Pe(\frac{\xi-z}{H})\}], & \xi \leq z \leq H \\ T_m, & 0 \leq z \leq \xi \end{cases} \quad (20)$$

The model defined by Equations 18, 19, 20 enables an estimate of ice temperature with depth, the existence of a temperate zone, and its thickness if one exists. Neither Meyer & Minchew (2018) nor our study accounts for geothermal heating in order to focus the study on the role of viscous dissipation, but it is feasible to represent the effects of geothermal heating through the boundary conditions of this thermomechanical model.

Meyer & Minchew (2018) apply this model to ice streams in Antarctica to show that active temperate zones may exist in many ice streams in Antarctica. However, we will recall that they assume $\Theta = 1$, thereby neglecting any other processes that may be resultant from the work done during ice deformation in shear margins. Here we seek to determine whether other processes may be significant and if this alters the estimates of ice temperature and temperate zones produced by Meyer & Minchew (2018), among other studies.

3. Steady State Grain Size Model

The steady-state grain size model was derived in Ranganathan et al. (2021) and follows the watt-meter derived by Austin & Evans (2007) and further explored and used

by Behn et al. (2009, 2020). Steady-state grain size is found by assuming three recrys-

tallization mechanisms - normal grain growth, rotation recrystallization, and migration

recrystallization - operate independently such that (Austin & Evans, 2007)

$$\dot{d} = \dot{d}_{rot} + \dot{d}_{mig} + \dot{d}_{nor} \tag{21}$$

The change in grain size due to normal grain growth is typically parameterized by (Alley

et al., 1986)

$$d_{\text{nor}}^p = d_0^p + kt \tag{22}$$

where d is grain size, d_0 is initial grain size, p is the grain-growth exponent, and k is

the grain growth rate. Rotation and migration recrystallization recrystallization are both

activated by deformation and alter surface and strain energy, respectively. Therefore, to

find the change in grain-size, we can estimate the change in surface and strain energy that

occurs as ice deforms. Rotation recrystallization alters the surface energy by subdividing

grains, and therefore the change in surface energy due to rotation recrystallization is found

by (Austin & Evans, 2007)

$$\dot{E}_{\text{surface}} = \frac{-c\gamma}{d^2}\dot{d}_{rot} \tag{23}$$

where c is a geometric constant, d is grain-size, and γ is grain-boundary energy. Migration

recrystallization alters strain energy by annihilating dislocations. The change in strain

energy and grain size due to migration recrystallization is derived by Ranganathan et al.

(2021) as

$$\dot{E}_{\text{strain}} = -\frac{1}{2}\frac{\tau_s^2}{\mu}\frac{p}{2}\frac{D^{\frac{p}{2}}}{d^{\frac{p}{2}+1}}\dot{d}_{mig} \tag{24}$$

$$\dot{d}_{\text{strain}} = MF_{mig} = \frac{1}{2}\frac{\tau_s^2}{\mu}\frac{D^{\frac{p}{2}}}{d^{\frac{p}{2}}}M \tag{25}$$

where τ is deviatoric shear stress, μ is the shear modulus, p is the grain-growth exponent, M is grain-boundary mobility, and D is a characteristic length-scale. Equations 23 and 24 can be applied to estimate $\dot{d}_{\text{rot}}$ by applying the equation for non-thermal energy found in Text S1 ($E_{\text{non-thermal}} = E_{\text{surface}} - E_{\text{strain}}$) and noting that $\dot{E}_{\text{non-thermal}} = (1 - \Theta)\tau_{ij}\dot{\epsilon}_{ij}$. Then, we can apply this to Equation 21 to find steady-state grain size:

$$d_{ss} = \left[\frac{\overbrace{4kp^{-1}c\gamma\mu^2}^{\text{Normal grain growth}} + \overbrace{\tau_s^4 D^p\left(\frac{p}{2}\right)M}^{\text{Migration recrystallization}}}{\underbrace{8(1-\Theta)\tau_s\dot{\epsilon}_s\mu^2}_{\text{Rotation Recrystallization}}} \right]^{\frac{1}{1+p}} \tag{26}$$

4. Computing Θ

To accurately predict ice temperature, the presence of temperate zones, and grain-sizes in shear margins, we must constrain Θ, the fraction of deformational work that is dissipated as heat, to gather a more complete understanding of the energy budget in glacier shear margins. We consider the balance of energy density in a given control volume between thermal energy density, surface and grain-boundary energy density, and elastic strain energy density, such that Θ can be written as

$$\Theta(\dot{\epsilon}, D, p, n) = \frac{|\dot{E}_{\text{thermal}}(\Theta, \dot{\epsilon}, n, T(\Theta, \dot{\epsilon}, n))|}{|\dot{E}_{\text{thermal}}(\Theta, \dot{\epsilon}, n, T(\Theta, \dot{\epsilon}, n))| + |\dot{E}_{\text{surface}}(d(\Theta, \dot{\epsilon}, D, p, n))| + |\dot{E}_{\text{strain}}(d(\Theta, \dot{\epsilon}, D, p, n), D, p, T(\Theta, \dot{\epsilon}, n}} \tag{27}$$

where $\dot{E}_{\mathrm{thermal}}$ represents the change in internal energy density due to change in thermal energy density due to viscous dissipation, $\dot{E}_{\mathrm{surface}}$ represents the change in surface energy density due to the reduction in grain size during rotation recrystallization, and $\dot{E}_{\mathrm{strain}}$ represents the change in elastic strain energy density due to migration recrystallization.

The increase in internal surface energy density due to the reduction in grain size is presented in Equation 23 and each of the terms are defined below. Note that during implementation, the rates of change are discretized ($\dot{E} \implies \Delta E$).

$$\dot{E}_{\mathrm{surface}} = \frac{-c\gamma}{d^2}\dot{d}_{\mathrm{rot}} \tag{28}$$

For example, for a discrete increase in grain size from about 2 mm at the surface to 40 mm at the bed, the magnitude of $\Delta E_{surface} \approx 10^3$ J m^{-3}. We approximate elastic strain energy from our interpretation of the dynamics occurring during migration recrystallization, so that that elastic strain energy density can be approximated by the change in energy due to an increase in dislocation density (Equation 24):

$$\dot{E}_{\mathrm{strain}} = -\frac{1}{2}\frac{\tau_s^2}{\mu}\frac{D^{\frac{p}{2}}}{d^{\frac{p}{2}+1}}\dot{d}_{\mathrm{mig}} \tag{29}$$

For a discrete increase in grain size from 2 mm to 40 mm, the magnitude of $\Delta E_{strain} \approx 10^7$ J m^{-3} for $\mu = 3e9$ Pa, $D = 0.05$ m, $p = 9$. Finally, the change in thermal energy density can be found by

$$\dot{E}_{\mathrm{thermal}} = \rho_i c_p \dot{T} \tag{30}$$

:

Since for ice, $\rho_i \approx 917$ kg m^{-3} and $c_p \approx 2000$ J kg^{-1} K^{-1} (Giauque & Stout, 1936), for a discrete increase in temperature from 248 K to 273 K, the magnitude $\Delta E_{thermal} \approx 10^7$ J m^{-3}.

Since these internal energies are dependent upon temperature and grain size, which are both dependent upon Θ, Equation 27 becomes a nonlinear equation that is solved using the Trust-Region-Dogleg method.

4.1. Binary Behavior of Θ

In nearly every case of strain rate and n value, there are two distinct solutions for different p and D values, because in almost all cases, E_{surface} is much less than E_{strain} and in some cases E_{surface} is much less than E_{strain}. If these two criteria are true, we can rewrite Equation 27 as

$$\Theta = \left[1 + \frac{\Delta E_{\text{strain}}}{\Delta E_{\text{thermal}}} \right]^{-1} \tag{31}$$

Thus, when $\frac{\Delta E_{\text{strain}}}{\Delta E_{\text{thermal}}} << 1$, $\Theta = 1$ and otherwise, $\Theta < 1$. From Equations 29 and 30, $\Theta = 1$ when

$$\frac{-\frac{1}{2} \frac{\sigma_s^2}{\mu} \frac{D^{\frac{p}{2}}}{d^{\frac{p}{2}+1}} \Delta d}{\rho_i c_p \Delta T} << 1 \tag{32}$$

Considering general values of grain size ($\sim \mathcal{O}(10\text{mm})$), temperature ($\sim 255 - 270\text{K}$), shear modulus ($3 \times 10^9$ Pa), and stress ($\sim \mathcal{O}(10^5\text{Pa})$), this simplifies to $\Theta = 1$ when

$$(\frac{D}{d})^{\frac{p}{2}} << 10^7 \tag{33}$$

Equation 33 provides the basis for Θ being binary. When, for example, $p \approx 2$, Equation 33 holds and $\Theta = 1$ for all strain rates. However, when $p \approx 9$, $(\frac{D}{d})^{\frac{p}{2}} \approx 10^7$ and $\Theta < 1$. This binary behavior of Θ allows us to completely map the possible values of Θ in glacier shear margins by considering two cases: Regime A (in which $D = 0.05$ and $p = 2$) and Regime B (in which $D = 0.05$ and $p = 9$). These two regimes cover the possible values of Θ for varying values of D and p.

5. Estimates of Θ for a Full Parameter Space

Equation 26 gives a steady-state grain size model, dependent on the fraction of work that is dissipated as heat in deforming glacier ice (the parameter Θ). We use the thermo-mechanical model derived by Meyer & Minchew (2018) to compute ice temperature, with Θ accounted for in the Brinkmann number (the ratio of heating to conduction). Both models assume steady-state creep, and the full ice column of shear margins are likely in steady state due to the speed of deformation driving a short time (< 10 years) to steady state.

This parameter Θ is currently unknown but controls both the steady state ice temperature and the steady state grain size. Figure S1 presents profiles of ice temperature and grain size for varying Θ. We show the variation in temperature and grain size profiles for ranges of reasonable strain rates seen within Antarctic ice streams (excluding very large or very small strain rates).

The fraction Θ controls how much ice temperature increases with increasing strain rate and, consequently, how much grain sizes grow. The grain size at the bed is largely controlled by Θ, the characteristic length scale D, and the grain-growth exponent p. As Θ decreases, zones of temperate ice disappear and temperature and grain size profiles ap-

proach approximately constant values with depth ($\Theta = 0.01$). Furthermore, strain rates play a significant role in determining the magnitude of grain growth and temperature increases. For large strain rates (dotted lines), temperate zones remain quite large for smaller Θ and grains becomes coarse rapidly ~ 30 mm. However, for low strain rates (dashed lines), grains remain roughly constant with temperature for all Θ and temperatures never reach the melting point, even for $\Theta = 0.99$. Finally, for moderate strain rates (solid lines), a zone of temperate ice forms for $\Theta = 0.99$ but for $\Theta <\sim 0.9$, the temperate zone disappears. The most dramatic grain growth occurs for moderate strain rates at approximately halfway down the ice column.

The rapid growth of grains is due to temperatures approaching $-10°$C, when enough strain energy has built for grain boundaries to migrate through migration recrystallization. Below approximately 500 meters height above the bed, grain sizes become roughly constant with depth, due to strain and temperature increasing enough such that creep and subsequent grain reduction due to rotation recrystallization becomes more active. Once ice temperature reaches the melting point and temperate zones form, recrystallization processes likely change due to the presence of significant liquid water in between grain boundaries. This liquid water likely makes grain boundaries even more mobile, encouraging coarsening of grains. Extremely coarse grains have been found in temperate glaciers (Tison & Hubbard, 2000), though further theoretical and experimental work is needed to consider in depth the effect that recrystallization may have on temperate ice.

The parameter Θ is dependent upon the values of D, the characteristic grain size, and p, the grain-growth exponent, as well as strain rate and n, the exponent in the constitutive

relation. Figure S2 shows Θ for the full D-p parameter space, for varying strain rate and n.

The value of the flow-law exponent n describes the sensitivity of strain rates to stresses and generally corresponds to the mechanism of ice flow. Values higher than 3 suggest a dislocation-creep regime, in which ice flow occurs through line defects called dislocations (Goldsby & Kohlstedt, 1997). In an $n = 4$ regime, $\Theta = 1$ for high strain rates, suggesting that thermal energy is higher in magnitude than elastic strain energy for most cases except very high strain rates $\dot{\epsilon} \approx 10^{-8}$ s^{-1}, for large values of D (large characteristic length-scale for elastic strain energy), and for high values of p (large grain growth exponents). Thus, in an $n = 4$ regime, $\Theta < 1$ only for very rapidly deforming glaciers.

A constitutive relation with $n = 2$ corresponds to a flow regime in which the dominant creep mechanism is grain-boundary sliding (Goldsby & Kohlstedt, 1997). If $n = 2$, Θ becomes close to 0, suggesting very little heating, for almost all physically-reasonable strain rates. At very low strain rates ($\dot{\epsilon} \approx 10^{-10}$ s^{-1}), $\Theta \approx \frac{1}{5}$ for much of the parameter space, likely due to strain rates being so low that most deformation is not occurring. Values of the flow exponent closer to $n = 3$ more accurately describe a combination of dislocation creep and grain-boundary sliding, a mechanism that is grain-size dependent and generally occurs in fine-grained materials (Ashby, 1972).

Further, the boundary between the two regimes changes based on the value of n and the strain rate. In particular, for low strain rates, $\Delta E_{\text{elastic}}$ is low, and therefore it is not necessarily much greater than $\Delta E_{\text{surface}}$. Thus, the assumption made to simplify Equation 27 to Equation 31 does not necessarily hold. This results in a more diffuse boundary and less defined binary behavior.

6.   Results for Other Outlet Glaciers

Results for Bindschadler and MacAyeal Ice Stream are found in Figure S3 and results

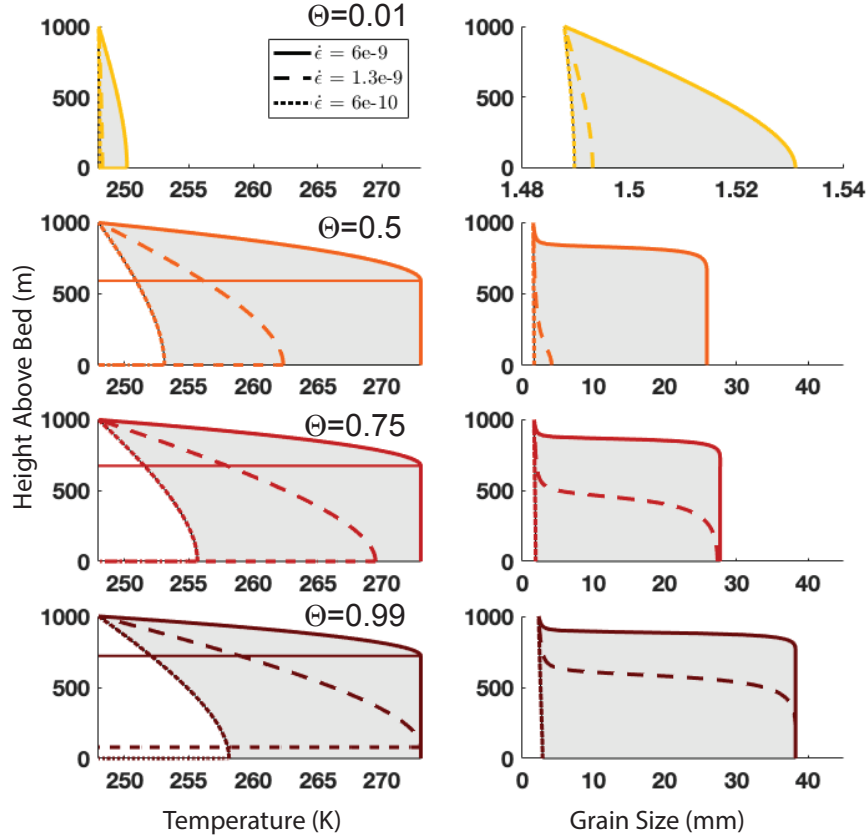for Byrd Glacier are found in Figure S4.

Figure S1. Ice temperature profiles, computed from the model derived in (Meyer & Minchew, 2018), and steady-state grain sizes profiles, computed from the model derived in this study, for varying values of Θ and varying lateral shear strain rates. A range of temperatures and grain sizes are plotted for low lateral shear strain rates ($\dot{\epsilon} = 6 \times 10^{-10}$ s^{-1}, dashed line), moderate strain rates ($\dot{\epsilon} = 1.3 \times 10^{-9}$ s^{-1}, solid line), and high strain rates ($\dot{\epsilon} = 6 \times 10^{-9}$ s^{-1}, dotted line). We use the constitutive relation to compute the work rate.
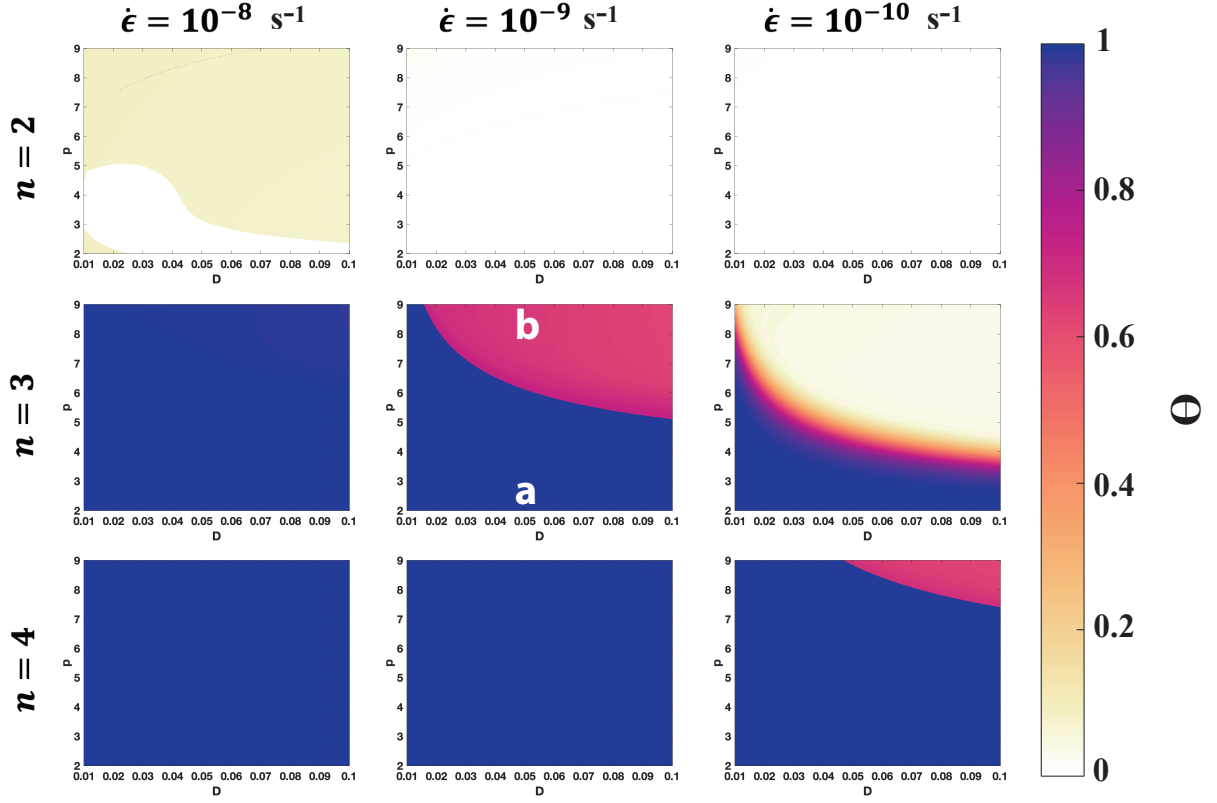
:

Figure S2. Estimated values of Θ for varying characteristic length scale for migration recrystallization, D, grain growth exponent, p, flow law exponent, n, and lateral shear strain rate. For most cases, there are two clear regimes for varying D and p, which we label Regime A and Regime B (middle panel).
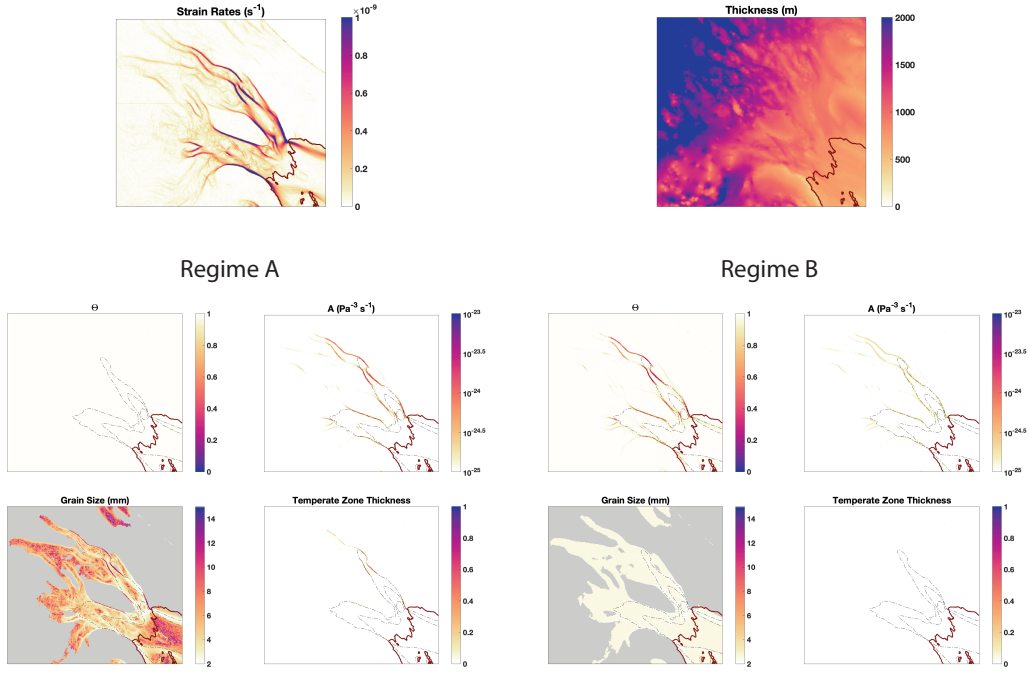
Figure S3.   Strain rates computed from surface velocity fields derived from Landsat 7 and 8 (Gardner et al., 2018) and thickness computed from REMA surface elevation (Howat et al., 2019) and BedMachine bed topography (Morlighem et al., 2020) in the first row. Second and third rows show estimated values of Θ, the depth-averaged flow-rate parameter, steady-state depth-averaged grain size, and the thickness of temperate zones as a fraction of ice thickness in Bindschadler and MacAyeal Ice Streams for both regimes (Regime A: $D = 0.05$ mm, $p = 2$, Regime B: $D = 0.05$ mm, $p = 9$).
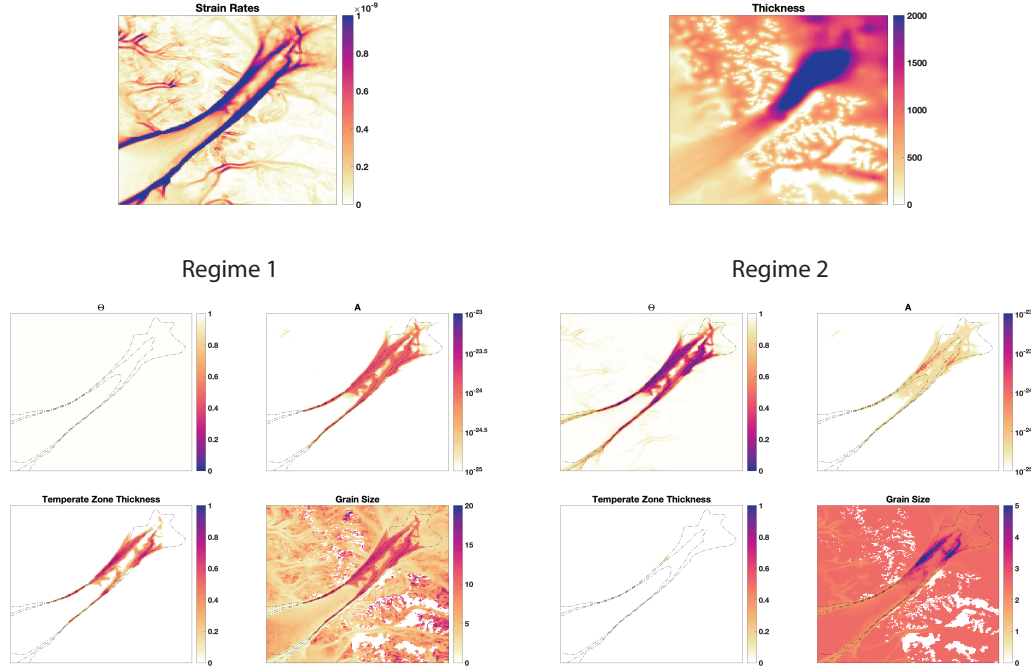
Figure S4.   Strain rates computed from surface velocity fields derived from Landsat

7 and 8 (Gardner et al., 2018) and thickness computed from REMA surface elevation

(Howat et al., 2019) and BedMachine bed topography (Morlighem et al., 2020) in the first

row. Second and third rows show estimated values of Θ, the depth-averaged flow-rate

parameter, steady-state depth-averaged grain size, and the thickness of temperate zones

as a fraction of ice thickness in Byrd Glacier for both regimes (Regime A: $D = 0.05$ mm,

$p = 2$, Regime B: $D = 0.05$ mm, $p = 9$).

References

Alley, R., Perepezko, J., & Bentley, C. (1986). Grain Growth in Polar Ice: I. Theory. *Journal of Glaciology*, *32*(112), 425–433. doi: 10.3189/s0022143000012132

Ashby, M. F. (1972). A first report on deformation-mechanism maps. *Acta Metallurgica*, *20*(7), 887–897. doi: 10.1016/0001-6160(72)90082-X

Austin, N. J., & Evans, B. (2007). Paleowattmeters: A scaling relation for dynamically recrystallized grain size. *Geology*, *35*(4), 343. Retrieved from `https://pubs.geoscienceworld.org/geology/article/35/4/343-346/129818` doi: 10.1130/G23244A.1

Behn, M. D., Goldsby, D. L., & Hirth, G. (2020). The role of grain-size evolution on the rheology of ice: Implications for reconciling laboratory creep data and the Glen flow law. *The Cryosphere Discussions*(November), 1–31. Retrieved from `https://tc.copernicus.org/preprints/tc-2020-295/` doi: 10.5194/tc-2020-295

Behn, M. D., Hirth, G., & Elsenbeck II, J. R. (2009, may). Implications of grain size evolution on the seismic structure of the oceanic upper mantle. *Earth and Planetary Science Letters*, *282*(1-4), 178–189. Retrieved from `http://dx.doi.org/10.1016/j.epsl.2009.03.014https://linkinghub.elsevier.com/retrieve/pii/S0012821X09001575` doi: 10.1016/j.epsl.2009.03.014

De Bresser, J. H. P., Peach, C. J., Reijs, J. P. J., & Spiers, C. J. (1998, sep). On dynamic recrystallization during solid state flow: Effects of stress and temperature. *Geophysical Research Letters*, *25*(18), 3457–3460. Retrieved from `http://doi.wiley.com/10.1029/98GL02690` doi: 10.1029/98GL02690

De La Chapelle, S., Castelnau, O., Lipenkov, V., & Duval, P. (1998, mar). Dynamic recrystallization and texture development in ice as revealed by the study of deep ice cores in Antarctica

and Greenland. *Journal of Geophysical Research: Solid Earth*, *103*(B3), 5091–5105. Retrieved from `http://doi.wiley.com/10.1029/97JB02621` doi: 10.1029/97JB02621

Derby, B. (1992, dec). Dynamic recrystallisation: The steady state grain size. *Scripta Metallurgica et Materialia*, *27*(11), 1581–1585. Retrieved from `https://linkinghub.elsevier.com/retrieve/pii/0956716X92901488` doi: 10.1016/0956-716X(92)90148-8

Derby, B., & Ashby, M. (1987, jun). On dynamic recrystallisation. *Scripta Metallurgica*, *21*(6), 879–884. Retrieved from `https://linkinghub.elsevier.com/retrieve/pii/0036974887903413` doi: 10.1016/0036-9748(87)90341-3

Gardner, A. S., Moholdt, G., Scambos, T., Fahnstock, M., Ligtenberg, S., van den Broeke, M., & Nilsson, J. (2018, feb). Increased West Antarctic and unchanged East Antarctic ice discharge over the last 7 years. *The Cryosphere*, *12*(2), 521–547. Retrieved from `https://tc.copernicus.org/articles/12/521/2018/` doi: 10.5194/tc-12-521-2018

Giauque, W. F., & Stout, J. W. (1936, jul). The Entropy of Water and the Third Law of Thermodynamics. The Heat Capacity of Ice from 15 to 273K. *Journal of the American Chemical Society*, *58*(7), 1144–1150. Retrieved from `https://pubs.acs.org/doi/abs/10.1021/ja01298a023` doi: 10.1021/ja01298a023

Goldsby, D. L., & Kohlstedt, D. L. (1997). Flow of ice by Dislocation, Grain Boundary Sliding, and Diffusion Processes. *Lunar and Planetary Science*.

Howat, I. M., Porter, C., Smith, B. E., Noh, M.-J., & Morin, P. (2019, feb). The Reference Elevation Model of Antarctica. *The Cryosphere*, *13*(2), 665–674. Retrieved from `https://tc.copernicus.org/articles/13/665/2019/` doi: 10.5194/tc-13-665-2019

Meyer, C. R., & Minchew, B. M. (2018, sep). Temperate ice in the shear margins of the Antarctic Ice Sheet: Controlling processes and preliminary locations. *Earth and Planetary Science Let-*

ters, *498*, 17–26. Retrieved from `https://doi.org/10.1016/j.epsl.2018.06.028https://linkinghub.elsevier.com/retrieve/pii/S0012821X18303790` doi: 10.1016/j.epsl.2018.06.028

Montagnat, M., & Duval, P. (2000, nov). Rate controlling processes in the creep of polar ice, influence of grain boundary migration associated with recrystallization. *Earth and Planetary Science Letters*, *183*(1-2), 179–186. Retrieved from `https://linkinghub.elsevier.com/retrieve/pii/S0012821X00002624` doi: 10.1016/S0012-821X(00)00262-4

Montagnat, M., & Duval, P. (2004). Dislocations in ice and deformation mechanisms: From single crystals to polar ice. *Defect and Diffusion Forum*, *229*(January 2017), 43–54. doi: 10.4028/www.scientific.net/ddf.229.43

Morlighem, M., Rignot, E., Binder, T., Blankenship, D., Drews, R., Eagles, G., ... Young, D. A. (2020). Deep glacial troughs and stabilizing ridges unveiled beneath the margins of the Antarctic ice sheet. *Nature Geoscience*, *13*(2), 132–137. Retrieved from `http://dx.doi.org/10.1038/s41561-019-0510-8` doi: 10.1038/s41561-019-0510-8

Ranganathan, M., Minchew, B., Meyer, C., & Pec, M. (2021). *Recrystallization of ice enhances the creep and vulnerability to fracture of ice shelves.* doi: 10.31223/X5W31W

Rollett, A. D., & Kocks, U. (1993). A Review of the Stages of Work Hardening. *Solid State Phenomena*, *35-36*(January), 1–18. doi: 10.4028/www.scientific.net/ssp.35-36.1

Tison, J. L., & Hubbard, B. (2000). Ice crystallographic evolution at a temperate glacier: Glacier de Tsanfleuron, Switzerland. *Geological Society Special Publication*, *176*, 23–38. doi: 10.1144/GSL.SP.2000.176.01.03

Wenk, H. R., Canova, G., Bréchet, Y., & Flandin, L. (1997). A deformation-based model for recrystallization of anisotropic materials. *Acta Materialia*, *45*(8), 3283–3296. doi: 10.1016/

S1359-6454(96)00409-0

Wilson, C. J., & Zhang, Y. (1996). Development of microstructure in the high-temperature deformation of ice. *Annals of Glaciology*, *23*, 293–302. doi: 10.3189/s0260305500013562